Low Free Energy Surfaces Using Blends of Fluorinated Acrylic Copolymer and Hydrocarbon Acrylic Copolymer Latexes

R. R. Thomas,*,† K. G. Lloyd,‡ K. M. Stika,‡ L. E. Stephans,*,§ G. S. Magallanes,⊥ V. L. Dimonie,⊥ E. D. Sudol,⊥ and M. S. El-Aasser*,⊥

Jackson Laboratory, E. I. du Pont de Nemours & Co., Deepwater, New Jersey 08023; E. I. du Pont de Nemours & Co., Corporate Center for Analytical Sciences, Experimental Station, Wilmington, Delaware 19880-0323; Department of Chemistry and Physics, Rowan University, Glassboro, New Jersey 08028; and Emulsion Polymers Institute and Department of Chemical Engineering, Lehigh University, Bethlehem, Pennsylvania 18015-4732

Received February 4, 2000; Revised Manuscript Received June 26, 2000

ABSTRACT: Blends of small particle size fluorinated acrylic copolymer latexes with a large particle size styrene/acrylic copolymer latex were examined with regard to formation of low free energy surfaces, amount of incorporated fluorinated copolymer, particle size, and particle size asymmetry. The styrene/acrylic latex was prepared by emulsion polymerization of *n*-butyl acrylate and styrene. Several varieties of fluorinated latexes were prepared. One was prepared by copolymerization of *n*-butyl acrylate and the fluorinated monomer, FMA, $H_2C{=}C(CH_3)CO_2(CH_2)_2(CF_2)_nF$ ($\bar{n} \approx 7.7$). Two types of copolymer core/fluorinated copolymer shell latex systems were prepared. One was comprised of a highly cross-linked core of poly(divinylbenzene) and a shell of poly(*n*-butyl acrylate-*co*-FMA). The other had a lightly cross-linked core of poly(*n*-butyl acrylate-*co*-divinylbenzene) and a shell of poly(*n*-butyl acrylate-*co*-FMA). Films cast from blends of styrene/acrylic and fluorinated copolymer latexes were examined by contact angle goniometry, X-ray photoelectron spectroscopy (XPS), time-of-flight static secondary ion mass spectroscopy (ToF-SIMS), and tapping mode atomic force microscopy (TMAFM). In some cases, low free energy surfaces were created at small mole fractions ($\sim 10^{-4}-10^{-2}$) of fluorinated monomer copolymerized with acrylic monomers in the mixture. AFM images were used to differentiate fluorinated, phase-segregated regions in the mixtures. Because of the disparity in particle size (asymmetry) between the styrene/acrylic and fluorine-containing latexes, the phenomena of percolation and excluded volume can be used to establish a substantial excess of fluorinated, low free energy material at the surface of an asymmetric blend of the two.

Introduction

Fluorochemicals are applied to reduce surface free energy and decrease wetting on many types of surfaces. The equation governing wetting on a surface was given by Young,

$$\gamma_l \cos\theta = \gamma_s - \gamma_{sl} \quad (1)$$

where γ refers to interfacial tension at liquid/air interface (l), solid/air interface (s), and solid/liquid interface (sl) and θ is the contact angle of a sessile liquid droplet resting on the solid surface.[1] It can be seen readily that a large contact angle is the result of a fluorochemical surface affording the lowest surface free energy (tension) of any commonly available material.

Fluorochemicals are typically copolymer systems that contain the perfluoroalkyl group ($-(CF_2)_nF$). The $-CF_3$ terminus on a pendant perfluoroalkyl chain provides much lower surface free energies than typical poly(tetrafluoroethylene)-like materials containing the $-CF_2-$ moiety in the polymer backbone.[2−4] Acrylic copolymers made of hydrocarbon and fluorocarbon monomers are used commonly to prepare low surface energy systems. Often the fluorochemical copolymer is part of a mixture of other co- or homopolymers. For practical reasons, the fluorochemical is delivered often from an aqueous system. To date, very few reports have appeared that detail studies of preparation and film formation of fluorine-containing latexes.[5,6] In a recent communication, details of film formation and synthesis of components used for blends of fluorinated and fluorine-free latexes were discussed.[7]

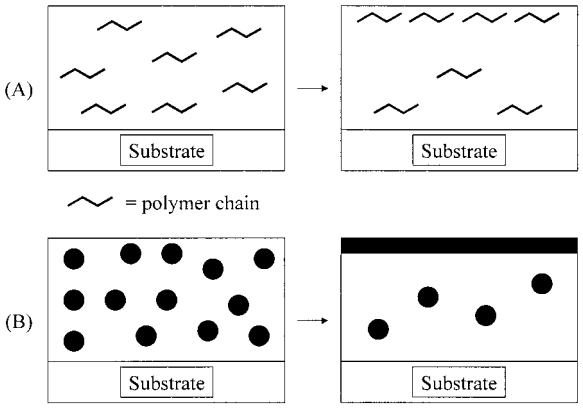

Figure 1. Comparison of methods to obtain low free energy surfaces. Depicted are surface segregation (A) of low free energy polymer chains and (B) phase separation of low free energy material in a matrix polymer.

To achieve a low surface free energy, the surface of a material needs to be covered with perfluoroalkyl groups. This leaves several options on the formulation of a low surface free energy system. Shown in Figure 1 are two phenomena that can be exploited to deliver low free

† Jackson Laboratory, E. I. du Pont de Nemours & Co.
‡ Corporate Center for Analytical Sciences, E. I. du Pont de Nemours & Co.
⊥ Lehigh University.
§ Rowan University.
* To whom correspondence should be addressed.

10.1021/ma000221p CCC: $19.00
Published on Web 10/21/2000

surface energy components to a surface. These are, namely, surface segregation and phase separation. Surface segregation relies on a differential of surface free energy between a fluorinated material and matrix as a force to drive the low free energy, fluorinated components to the surface and is observed with soluble fluorinated materials. The other method used to place low surface free energy, fluorinated material at a surface is phase separation driven by incompatibility of components in a mixture and is often the result of even larger free energy gradients between the two components.

Latexes containing fluorinated polymers can be used to prepare low free energy surfaces. Because of the presence of particles, multiple interfaces, and a wide range of components used in formulation, latex systems are inherently heterogeneous. The low free energy surface can be created through surface segregation or phase separation of fluorinated components to the surface. However, another phenomenon is possible with latex or heterogeneous systems. Statistically, fluorinated latex particles would be present on the film surface in an amount equal to their volume fraction in the bulk. This has the advantage that phase separation kinetics are unimportant, but the disadvantage that large and, often, prohibitive volume fractions of fluorinated latex would be required to achieve the greatest surface free energy reduction.

The disadvantages of using large volume fractions of fluorinated latex particles can be overcome by taking advantage of a situation that is unique with systems containing particles. Latex systems can offer a distinct advantage lacking with homogeneous delivery (soluble or compatible systems) such as found with solution polymers. Asymmetric (different particle size) mixtures can be used. In this fashion, the phenomenon of packing efficiency can be used to advantage allowing smaller particles to be in relative excess at a surface. Theoretically, a monodisperse collection of particles in a hexagonally close-packed array can occupy only ~74% of a planar, projected surface. If particles of various sizes are mixed, the packing efficiency increases accordingly since small particles can occupy the interstices between larger particles. The interstices extend to the surface. As a result, more of the small particle size latex is able to fill the surface. This observation has been noted previously in the work of Eckersley and Helmer using latex blends.[8] If the small particles contained a fluorinated copolymer, then they may be placed near a surface mechanically as opposed to allowing surface segregation or phase separation to enrich the surface in low free energy components. This scheme is depicted in Figure 2.

Although not necessary to obtain low free energy surfaces, connectivity of the fluorochemical latexes at the surface is advantageous from a surface coverage perspective. The concept of percolation deals with the dispersion of one phase in another,[9] such as in the present case. Various algorithms have been constructed to determine percolation thresholds for particle connectivity. Percolation has been employed successfully to prepare conductive polymers with very low volume fractions of conductive material in a mixture.[10−17] To date, no published work has addressed this phenomenon and its effect on surface excess of low free energy materials in asymmetric latex blends.

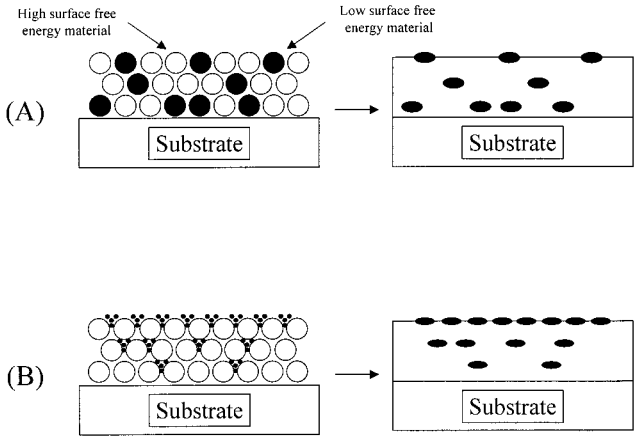

Figure 2. Effect of particle size asymmetry in formation of low free energy surfaces using particles of same size (A) and particles of different sizes (B).

Furthermore, asymmetric blends can offer another distinct advantage as a result of the excluded-volume effect. As an asymmetric blend becomes more concentrated (distance between large particles < diameter of small particle), an attractive potential is established between large particles that is equal to the osmotic pressure of the small particles in the excluded volume.[18−21] As a result, particles of similar diameter have a tendency to cluster leading, in essence, to a form of phase separation.[20,21]

Blends of latexes can be used to deliver low free energy, fluorinated components to a surface while minimizing the inherent shortcomings of diffusion, surface segregation, and phase separation. This report will detail findings using asymmetric blends of fluorinated acrylic copolymer latexes with a fluorine-free acrylic copolymer latex with regard to formation of low free energy surfaces, amount of incorporated fluorinated copolymer, particle size, and particle size asymmetry.

Experimental Section

General. The (perfluoroalkyl)ethyl methacrylate monomer ($H_2C{=}C(CH_3)CO_2(CH_2)_2(CF_2)_nF$) was obtained from E. I. du Pont de Nemours and Co. and is sold under the trade name ZONYL. The value of *n* ranges from 6 to 18 with the average ≈7.7. Sodium lauryl sulfate (SLS) was obtained from Fisher Scientific. Cetyl alcohol (CA), divinylbenzene, 80% active ingredient (DVB), *n*-butyl acrylate (BuA), styrene (S), and hexadecane were obtained from Aldrich Chemical Co. and used as received. Water was of deionized quality. Polystyrene molecular weight calibration standards were obtained from Pressure Chemical Co.

Preparation of Large Particle Size Poly(*n*-butyl acrylate-*co*-styrene) Latex 1 (BuA/S, 55/45 wt %). The synthesis of the poly(*n*-butyl acrylate-*co*-styrene) latex **1** was performed by a conventional emulsion polymerization process at 70 °C for 6−8 h. The recipe consisted of equimolar amounts of the two monomers *n*-butyl acrylate (16.03 g) and styrene (13.11 g) along with 3.64 g of a 5 wt % aqueous solution of sodium diamyl sulfosuccinate (Aerosol AY), 0.29 g of nonyl phenoxy polyoxyethylene ethanol (Igepal 880), 0.18 g of sodium bicarbonate, and potassium persulfate (0.18 g) as initiator in 117 g of distilled water.

Preparation of Small Particle Size Fluorinated Latex 2 (BuA/FMA, 98.6/1.4 wt %). The small particle size fluorinated latex, **2**, containing the fluorinated monomer was prepared by miniemulsion polymerization. The recipe consisted of *n*-butyl acrylate (20.49 g), FMA (6.84 g), sodium lauryl sulfate (0.50 g, 10 mmol on water), cetyl alcohol (1.67 g, 40 mmol on water), and potassium persulfate (0.092 g, 2 mmol on water) as initiator in 171 g of distilled water. The polym-

erization scheme consisted of mixing sodium lauryl sulfate and cetyl alcohol into the aqueous phase at 70 °C for 30 min and then cooled to room temperature. The monomers were mixed separately as the oil phase. The aqueous and oil phases were mixed for 30 min at room temperature followed by sonification for 1 min and then passed through a microfluidizer (Microfluidics model 110T) for 15 cycles. Potassium persulfate initiator solution was added, and the miniemulsion polymerization was performed at 70 °C for 8−10 h.

Preparation of Small Particle Size Core/Fluorinated Shell Latex 3 (DVB Core/(BuA/FMA Shell, 82/18 wt %). The core/shell latex, **3**, containing a poly(divinylbenzene) core and poly(*n*-butyl acrylate-*co*-FMA) shell was made by preparing a small particle size latex similar to **2** except that divinylbenzene (27.30 g) was used in place of the *n*-butyl acrylate/FMA mixture. The small particle size latex thus obtained was used as a seed for making the core/shell latex. The aqueous seed latex (150 g, ∼14.6 wt % solids) was placed in flask, heated to 70 °C, and purged with nitrogen. Potassium persulfate (0.092 g) initiator was added to the reaction mass prior to addition of monomers. The *n*-butyl acrylate (3.64 g)/FMA (3.64 g) mixture was added continuously to the latex seed over a period of 4 h. The reaction temperature was maintained for at least 1 h after the monomer feed ended.

Preparation of Small Particle Size Core/Fluorinated Shell Latex 4 (BuA/DVB Core, 85/15 wt %)/(BuA/FMA Shell, 92/8 wt %). The core/shell latex, **4**, containing a poly(*n*-butyl acrylate-*co*-divinylbenzene) core and poly(*n*-butyl acrylate-*co*-FMA) shell was made by preparing a small particle size latex similar to **2** except that divinylbenzene (5.36 g) and *n*-butyl acrylate (22.20 g) were used in place of the *n*-butyl acrylate/FMA mixture. The small particle size latex thus obtained was used as a seed for the shell latex. The aqueous seed latex (150 g, ∼14.6 wt % solids) was placed in flask, heated to 70 °C, and purged with nitrogen. Potassium persulfate (0.092 g) initiator was added to the reaction mass prior to addition of monomers. The *n*-butyl acrylate (7.61 g)/FMA (2.54 g) mixture was added continuously to the latex seed over a period of 4 h. The reaction temperature was maintained for at least 1 h after the monomer feed ended.

Preparation of Latex Blend and Pure Films. Films of the blends and pure materials were prepared by dip-coating on glass slides from freshly stirred solutions. The films were allowed to dry at room temperature overnight before subsequent analysis. The glass slides were cleaned with acetone and then allowed to soak in 5 wt % aqueous NaOH for 1 h followed by extensive rinsing with distilled water and drying at room temperature. Film thicknesses were measured by profilometry using a Sloan Dektak 3030.

Contact Angle Measurements. Contact angle measurements were performed using a VCA-2500 contact angle goniometer from AST Products (Billerica, MA). The device uses a CCD camera, frame grabber, and software to capture the contact angle image. Typically, measurements were collected for four drops across the surface. The standard deviations are shown in the contact angle figures. Advancing contact angles were determined by expanding the droplet on the surface until an equilibrium angle was observed. Receding angles were obtained by removing liquid from the droplet until its base contracted and an equilibrium angle was seen.

X-ray Photoelectron Spectroscopy. XPS data were collected in both survey and high-resolution mode on Phi LS5000 and 5400 systems equipped with a Mg anode operating at 300 W. Typical analysis areas were 2 × 8 mm. Data were recorded at both 30° and 90° collection angles, resulting in analysis depths of ∼50 and 100 Å, respectively. Quantification was done by integration of the atomic signals and corrected with Scofield sensitivity factors adjusted for the instrument lens and detector design. The element-specific detection limit was on the order of 0.5 atom %.

Atomic Force Microscopy. Atomic force microscopy was performed using a Dimension 3100 instrument (Digital Instruments, Santa Barbara, CA). Images were acquired under ambient conditions in tapping mode using a Nanoprobe cantilever (125 μm length with a typical resonance frequency of 298−366 kHz). Samples were prepared by placing a small droplet (∼10−20 μL) of the stirred latex on the surface of freshly cleaved ruby mica and allowed to dry at room temperature in air for at least 1 day. Unless stated otherwise, images were acquired in the light (set-point ratio ≈ 0.8−0.9) tapping mode.

ToF-SIMS Analysis. ToF-SIMS experiments were carried out under ultrahigh vacuum with a Physical Electronics (PHI) model 7200 reflector-design time-of-flight mass spectrometer. An 8 keV bunched cesium primary ion source was used to generate the spectroscopic data, while a gallium liquid metal ion source, operated at 15−25 keV in unbunched mode, was used for secondary ion mapping experiments. Charge buildup at the insulating sample surface was compensated by use of a pulsed electron flood gun.

Thermal Analysis. Differential scanning calorimetry was performed using a TA Instruments DSC 2920. The samples were scanned from −50 to 300 °C at 10 °C/min for the heating cycle and the reverse for cooling. Sample decomposition was noted at 200−300 °C, so the scan was repeated on a fresh sample to just below the onset of decomposition. Samples for analysis were prepared from the pure latex or appropriate blends by drying for several days under vacuum at room temperature. No attempt was made to remove the surfactant(s) used in their preparation.

Particle Size Measurements. Latex volume average particle size measurements were performed by the capillary hydrodynamic fractionation technique using a CHDF-1000 instrument from Matec Applied Sciences.

Molecular Weight Determination. Molecular weights were determined using a Waters Associates gel permeation chromatograph employing two Waters Associates HR-4E columns and refractive index detection. Molecular weights are reported relative to polystyrene standards. Samples of the aqueous latex were dispersed in THF and allowed to stir for several hours permitting the polymer to dissolve.

Particle Density. Particle densities were determined using a Mettler/Paar DMA46 densiometer. Samples were diluted and densities determined from a plot of density vs weight percent solids after extrapolation to 100 wt %. Good correlation (r > 0.99) was observed with the data.

Fluorine Analysis. Fluorine analysis was performed by combustion analysis of the dried latexes using a modification[22] of the Wickbold method.[23]

Results and Discussion

Preparation of Latexes. Several different types of latexes were prepared. The hydrocarbon latex used as the matrix **1**, consisting of a *n*-butyl acrylate (BuA)/styrene (S) copolymer (55/45 wt %) was prepared by a conventional emulsion polymerization process using potassium persulfate as the initiator. The surfactants, sodium diamyl sulfosuccinate (Aerosol AY) and nonyl phenoxy polyoxyethylene ethanol (Igepal 880), were used to stabilize the latex. The fluorinated portion of the latex blend consisted of a (i) copolymer, **2**, of *n*-butyl acrylate and the perfluoroalkylethyl methacrylate monomer (FMA), $H_2C{=}C(CH_3)CO_2(CH_2)_2(CF_2)_nF$, (98.6/1.4 wt %, $\bar{n} \approx 7.7$), or (ii) a core/shell latex containing the fluorinated monomer copolymerized in the shell. The core/shell latexes were prepared with (i) divinylbenzene (DVB) **3** or (ii) *n*-butyl acrylate/divinylbenzene (85/15 wt %) **4** as the core. The shell was comprised of poly(*n*-butyl acrylate-*co*-FMA) (82/18 wt % for latex **3** or 92/8 wt % for latex **4**). The core latexes were prepared by miniemulsion polymerization using potassium persulfate as initiator and sodium lauryl sulfate as surfactant at 70 °C using cetyl alcohol (CA) or hexadecane (HD) as costabilizers. Particle sizes were smaller (55 nm) when CA was used as a costabilizer compared to 150 nm when HD was used. Therefore, the smaller particles

Table 1. Properties of Latexes

latex[a]	vol av particle diameter, D_v (nm)	particle size polydispersity index	M_w	M_n	dispersity M_w/M_n	ρ (g/mL)
BuA/S (55/45 wt %) **1**	412	1.00	299 000	53 400	5.7	1.079 ± 0.003
BuA/FMA (98.6/1.4 wt %) **2**	64.2	1.05	293 000	59 700	4.9	1.117 ± 0.003
DVB (core)/BuA/FMA (shell, 82/18 wt %) **3**	213	1.02	*b*	*b*	*b*	1.076 ± 0.003
DVB/BuA (core, 15/85 wt %)/BuA/FMA (shell, 92/8 wt %) **4**	122[c]	1.05	*b*	*b*	*b*	1.054 ± 0.002

[a] BuA ≡ *n*-butyl acrylate, S ≡ styrene, DVB ≡ divinylbenzene, and FMA ≡ CH_2=$C(CH_3)CO_2(CH_2)_2(CF_2)_nF$. [b] Insoluble in THF. [c] Bimodal.

were used as the core (seed) latex in a second stage polymerization to add a shell containing the fluorinated monomer. The composition of the fluorinated latexes was verified by fluorine analysis.

Latex Characterization, Film Formation, and Thermal Properties. Details regarding the characterization of latexes **1**−**4** are shown in Table 1. Films obtained by dip-coating on glass were in the thickness range 1−3 μm as measured by profilometry and appeared to be relatively smooth and continuous to the unaided eye. Samples were prepared for thermal analysis (differential scanning calorimetry, DSC) by drying the original latex without removing surfactant to mimic the conditions at which the films were formed. It has been demonstrated in a number of studies that the presence of surfactant can affect film formation and thermal transitions profoundly.[24,25] Unfortunately, the samples proved to be particularly unsuitable for thermal analysis. The fluorinated latex **2** (BuA/FMA, 98.6/1.4 wt %) exhibited a T_g at 11.1 °C with no apparent T_m. The fluorinated core/shell latex **3** (DVB core/(BuA/FMA shell, 82/18 wt %)) showed a T_g at 10.5 °C and a very broad thermal event at ∼240 °C, indicating the onset of decomposition. Homopolymers of FMA with monodisperse perfluoroalkyl chain lengths typically do not exhibit a T_g and have a T_m that is dependent on perfluoroalkyl chain length.[26] It is therefore not surprising to see complicated or an absence of meaningful thermal events with fluorine-containing materials due to dispersity introduced through a mixture of chain lengths.[27] The large particle size styrene/acrylic latex **1** (BuA/S, 55/45 wt %) had a T_g at 8.9 °C and exhibited no clear T_m. From the Fox equation,[28] the T_g of the hydrocarbon latex **1** can be estimated to be −4 °C. The difference of the T_g from its value predicted by the Fox equation has been demonstrated previously for statistical copolymers through plasticization or antiplasticization in the presence of surfactants, such as sodium diamyl sulfosuccinate or nonyl phenoxy polyoxyethylene ethanol used here.[24,25]

The fluorine content of the latexes was determined, in at least duplicate, by combustion analysis. Experimentally determined fluorine values were found to be low for all copolymers incorporating the FMA monomer compared to the polymerization recipe. For example, the recipe for the fluorinated latex **2** should have resulted in poly(*n*-butyl acrylate-*co*-FMA) with a weight ratio of 75% *n*-butyl acrylate-to-25% FMA instead of the 98.6% *n*-butyl acrylate-to-1.4% FMA weight ratio found for **2** (BuA/FMA, 98.6/1.4 wt %). The latex formulation given reflects quantities of FMA that were determined experimentally. Currently, no explanation can be provided for the diminished incorporation of the fluorinated monomer FMA into the copolymer during the polymerization process. One possibility is that FMA homopolymers or copolymers containing large mole fractions of FMA are excluded as a result of coagulum formation during polymerization. However, in the miniemulsion polymerization, insignificant (<1 wt %) amounts of coagulum are formed.

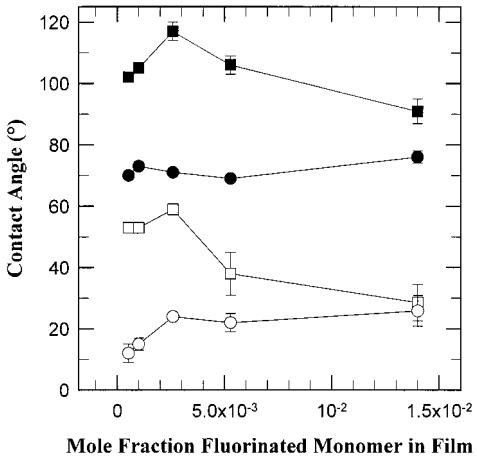

Figure 3. Water and hexadecane contact angle data for film obtained using a blend of the large particle size hydrocarbon latex **1** (BuA/S, 55/45 wt %) and the small particle size fluorinated latex **2** (BuA/FMA, 98.6/1.4 wt %). Advancing and receding water contact angles indicated by ■ and □, respectively. Advancing and receding hexadecane contact angles indicated by ● and ○, respectively.

Contact Angles. Shown in Figure 3 are water and hexadecane contact angle data on films cast from a blend of the large particle size latex **1** (BuA/S, 55/45 wt %) and the small particle size latex **2** (BuA/FMA, 98.6/1.4 wt %). At a fluorinated monomer mole fraction, χ_{FMA}, of 2.6 × 10^{-3}, water and hexadecane contact angles (∼120° and ∼60°, respectively) are approaching theoretical maxima for $-CF_3$ dominated surfaces (∼125° and ∼80°).[3,29,30] Conversely, water and hexadecane advancing contact angles on a surface cast from the pure latex **1** (BuA/S, 55/45 wt %) are 86° and 0°, respectively. Cassie derived an equation relating contact angles measured on surfaces of a binary mixture to fractional area occupied and intrinsic contact angles of the two pure components[31]

$$\cos\theta = f_1 \cos\theta_1 + f_2 \cos\theta_2 \qquad (2)$$

where θ is the observed contact angle, f_1 and f_2 are fractional area occupation of components 1 and 2, respectively, and θ_1 and θ_2 are the contact angles on pure components 1 and 2, respectively. Using hexadecane contact angles on the fluorinated and hydrocarbon components to be 80° and 0°, respectively, an estimate can be made that the surface area fraction occupied by the fluorinated component is ≈80%.

Contact angle data for a film obtained by blending latex **1** (BuA/S, 55/45 wt %) and small particle size core/shell latex **4** (BuA/DVB core, 85/15 wt %)/(BuA/FMA shell, 92/8 wt %) are given in Figure 4. While the contact angles are not as high as that for the mixture of **1** (BuA/S, 55/45 wt %) and **2** (BuA/FMA, 98.6/1.4 wt %) shown

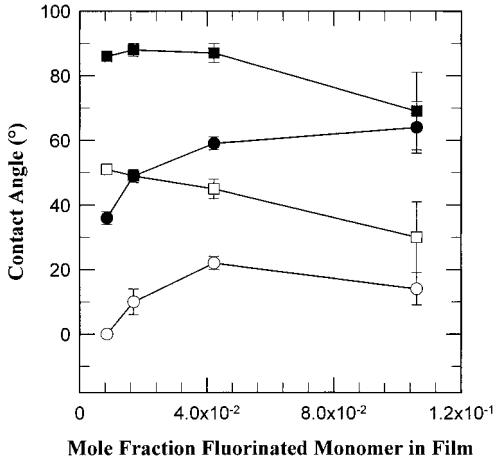

Figure 4. Water and hexadecane contact angle data for a film obtained by blending the large particle size hydrocarbon latex **1** (BuA/S, 55/45 wt %) and the small particle size fluorinated core/shell latex **4** (BuA/DVB core, 85/15 wt %)/(BuA/FMA shell, 92/8 wt %). Advancing and receding water contact angles indicated by ■ and □, respectively. Advancing and receding hexadecane contact angles indicated by ● and ○, respectively.

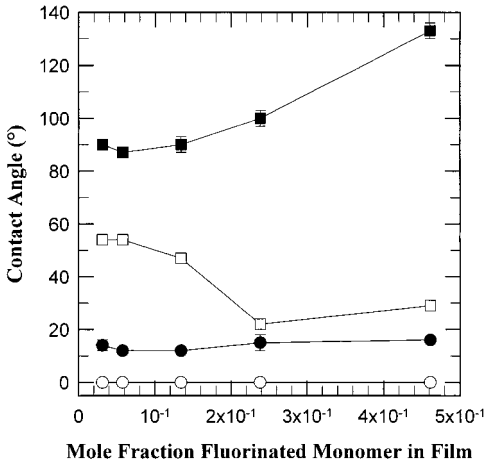

Figure 5. Water and hexadecane contact angle data for a film obtained by blending the large particle size hydrocarbon latex **1** (BuA/S, 55/45 wt %) and the small particle size fluorinated latex **3** (DVB core/(BuA/FMA shell, 82/18 wt %)). Advancing and receding water contact angles indicated by ■ and □, respectively. Advancing and receding hexadecane contact angles indicated by ● and ○, respectively.

in Figure 3, surface coverage of fluorine is appreciable and can be estimated to be in the range 20−80% based on analysis of contact angle data using eq 2 with $2 \times 10^{-3} < \chi_{FMA} < 1 \times 10^{-1}$.

The contact angles measured on a mixture containing the large particle size latex **1** (BuA/S, 55/45 wt %) and the core/shell latex **3** (DVB core/(BuA/FMA, 82/18 wt %)) are much lower than the two systems discussed previously and are shown in Figure 5. Hexadecane contact angles remain relatively low despite large amounts of fluorine in this film (mole fraction of FMA ≈ 10−100 × mole fraction of FMA in **2** (BuA/FMA, 98.6/1.4 wt %) or **4** (BuA/DVB core, 85/15 wt %)/(BuA/FMA shell, 92/8 wt %) based on pure latexes). Using eq 2, the surface coverage with low surface free energy, fluorinated material can be estimated to be 0−5% only.

It is well-known that surface roughness or chemical heterogeneity can cause contact angle hysteresis (difference between advancing and receding contact angles) and affect the value of the equilibrium Young contact angle (eq 1).[32−36] It is easy to imagine a case, such in the present, where both mechanisms may be operative. All contact angle data exhibit appreciable (∼0−100°, depending on sample) contact angle hysteresis. This is, undoubtedly, due in part to chemical heterogeneity of the different components at the surface. See, for example, Figures 5−10 and 12−15 and discussion of AFM results below. A detailed analysis of the effects of chemical heterogeneity on hysteresis is beyond the scope of this work. Suffice it to state that chemically heterogeneous surfaces exhibit contact angle hysteresis when components differ widely in surface free energy, and it is manifested in the current work.

The effect of surface roughness on apparent contact angles has been addressed by the equation due to Wenzel[37,38]

$$\cos \theta_{eff} = r \cos \theta \qquad (3)$$

where θ_{eff} is the measured contact angle and r is the ratio of true-to-planar surface area. The effect of surface roughness on contact angles can be estimated easily for one sample used in the current study. From geometrical arguments, $r \approx 1.4$ for a hexagonally close-packed array of latex **1** (BuA/S, 55/45 wt %) as shown in Figure 6. Solution of eq 3 yields $\theta \approx 88°$ compared to the measured $\theta_{eff} \approx 87°$. Because of the sine function, the deviation of θ from θ_{eff} will increase with decreasing contact angles. The effect of chemical heterogeneity and roughness in tandem on the equilibrium contact angle is not yet established firmly; however, in work by Swain and Lipowsky, an equation was proposed to account for both roughness and chemical heterogeneity.[39] Solution of this equation would require knowledge of variables that are beyond this work. In summary, the surfaces prepared in the current study are both rough and chemically heterogeneous, and there may be marked differences between the measured and Young contact angles, especially at low values of θ.

XPS Studies. Surface composition was verified by XPS measurements. Experimental and theoretical elemental compositions are given in Table 2. Comparison of the experimental XPS composition data for a film of the large particle size hydrocarbon latex **1** (BuA/S, 55/45 wt %) blended with the small particle size fluorinated latex **2** (BuA/FMA, 98.6/1.4 wt %) with theoretical values demonstrates the surface to be dominated by the latter. This finding is in agreement with contact angle data that gives an estimate of 80% surface occupation by fluorinated material. A similar comparison for film containing a blend of latex **1** (BuA/S, 55/45 wt %) with core/shell latex **4** (BuA/DVB core, 85/15 wt %)/(BuA/FMA shell, 92/8 wt %) again indicates the surface to be dominated by the fluorine-containing copolymer. Likewise, there is good agreement with surface coverage estimates based on contact angles using eq 2. A blend film consisting of the latex **1** (BuA/S, 55/45 wt %) and the cross-linked core/shell latex **3** (DVB core/(BuA/FMA, 82/18 wt %)) showed a different composition than the previous samples. While the core/shell latex **3** (DVB core/(BuA/FMA, 82/18 wt %)) is rich in fluorinated monomer, the surface composition shows very little excess of fluorine. In fact, core/shell latex **3** (DVB core/(BuA/FMA shell, 82/18 wt %) demonstrated the smallest excess of fluorine at the surface compared to the other pure fluorinated latexes (∼8× vs ∼40× and ∼23× for latexes **2** (BuA/FMA, 98.6/1.4 wt %) and **4** (BuA/DVB

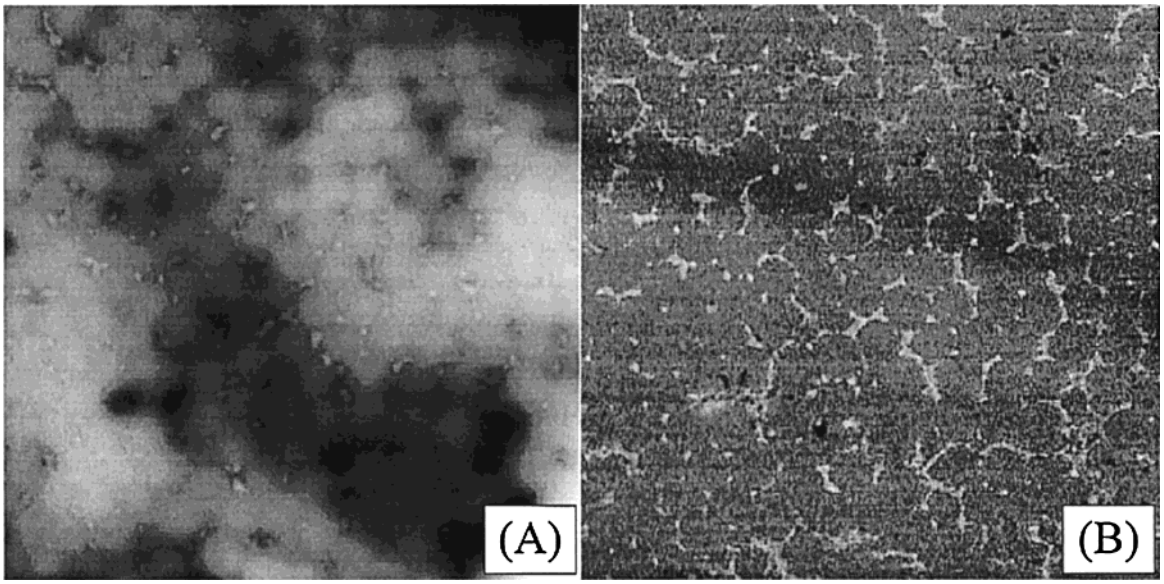

Figure 6. AFM height (A) and phase image (B) of pure hydrocarbon latex **1** (BuA/S, 55/45 wt %). The scan box is 5 μm × 5 μm. The height and phase scales are 0−100 nm and 0−30°, respectively, from dark to light color.

Table 2. XPS Data for Blends and Pure Latexes

sample[a]	take-off angle (deg)	atomic percentages C	O	F
1, BuA/S (55/45 wt %) theory		88	12	
1 experimental	90	79	19	
	30	78	20	
2, BuA/FMA (98.6/1.4 wt %) theory		77	22	0.63
pure **2** experimental	90	59	15	25
(mole fraction FMA copolymerized in film ≈ 1.4×10^{-2})	30	54	12	33
1 +BuA/FMA (98.6/1.4 wt %) **2**	90	65	16	18
(mole fraction FMA copolymerized in film ≈ 9.9×10^{-4})	30	57	12	30
3, (DVB core/(BuA/FMA shell, 82/18 wt %)) theory		96	3.0	1.2
pure **3** experimental	90	78	11	9.9
(mole fraction FMA copolymerized in film ≈ 4.6×10^{-1})	30	78	11	11
1 + (DVB core/(BuA/FMA shell, 82/18 wt %)) **3**	90	83	15	1.6
(mole fraction FMA copolymerized in film ≈ 1.3×10^{-1})	30	81	16	2.5
4, (BuA/DVB core, 85/15 wt %)/(BuA/FMA shell, 92/8 wt %) theory		81	18	0.64
pure **4** experimental	90	65	18	15
(mole fraction FMA copolymerized in film ≈ 1.1×10^{-1})	30	58	14	26
1 + (BuA/DVB core, 85/15 wt %)/(BuA/FMA shell, 92/8 wt %) **4**	90	69	21	4.3
(mole fraction FMA copolymerized in film ≈ 1.7×10^{-2})	30	69	20	7.9

[a] BuA ≡ *n*-butyl acrylate, S ≡ styrene, DVB ≡ divinylbenzene, and FMA ≡ $CH_2{=}C(CH_3)CO_2(CH_2)_2(CF_2)_nF$.

core, 85/15 wt %)/(BuA/FMA shell, 92/8 wt %), respectively). In addition, fluorine atomic percentages for core/shell latex **3** (DVB core/(BuA/FMA, 82/18 wt %)) collected at 30° and 90° takeoff angles are identical within instrumental error. In contrast, fluorinated latexes **2** (BuA/FMA, 98.6/1.4 wt %) and **4** (BuA/DVB core, 85/15 wt %)/(BuA/FMA shell, 92/8 wt %) exhibit fluorine atomic percentages that are a factor of 1.5−2 times greater for data collected at 30° than at 90°. The apparent lack of fluorinated material delivered to the surface using latex **3** (DVB core/(BuA/FMA shell, 82/18 wt %) can be explained by morphology of the resultant composite particle to be discussed in a later section.

For asymmetric mixtures of **2** (BuA/FMA, 98.6/1.4 wt %) or **4** (BuA/DVB core, 85/15 wt %)/(BuA/FMA shell, 92/8 wt %) with latex **1** (BuA/S, 55/45 wt %), XPS data collected at 90° (Table 2) show the surface to be in substantial excess of fluorine and well above bulk levels. Under the present experimental conditions (Mg Kα radiation), this would correspond to an integrated sampling depth ≈100 Å and indicate a thickness of the fluorochemical layer greater than a monolayer. At a more shallow takeoff angle of 30°, the XPS data for fluorinated latexes **2** (BuA/S, 98.6/1.4 wt %) and core/shell latex **4** (BuA/DVB core, 85/15 wt %)/(BuA/FMA shell, 92/8 wt %) as well as their blends with hydrocarbon latex **1** (BuA/S, 55/45 wt %) exhibit an even larger excess of fluorine at the surface than for data collected at 90°.

Time-of-Flight Secondary Ion Mass Spectroscopy. Latex surfaces were also examined by time-of-flight secondary ion mass spectroscopy (ToF-SIMS) in an effort to verify the data from contact angle goniometry and XPS. Discovered in a previous study, the perfluoroalkylethyl methacrylate monomer in a copolymer yields a rich and abundant negative ion spectrum due to the production of an acetylide fragment upon sputtering (cleavage between C^1 and C^2 with loss of 2HF).[40] Due to dispersity of perfluoralkylethyl chain lengths in the FMA monomer, fluorinated acetylide fragments are observed at 293, 393, 493, ..., *m*/*z* (loss of $(-CF_2CF_2-)_n$.)

$$-C(=O)OC^1H_2C^2H_2C^3F_2C^4F_2\cdots C^xF_2F \xrightarrow{-2HF} -C{\equiv}C-(CF_2)_{x-3}F$$

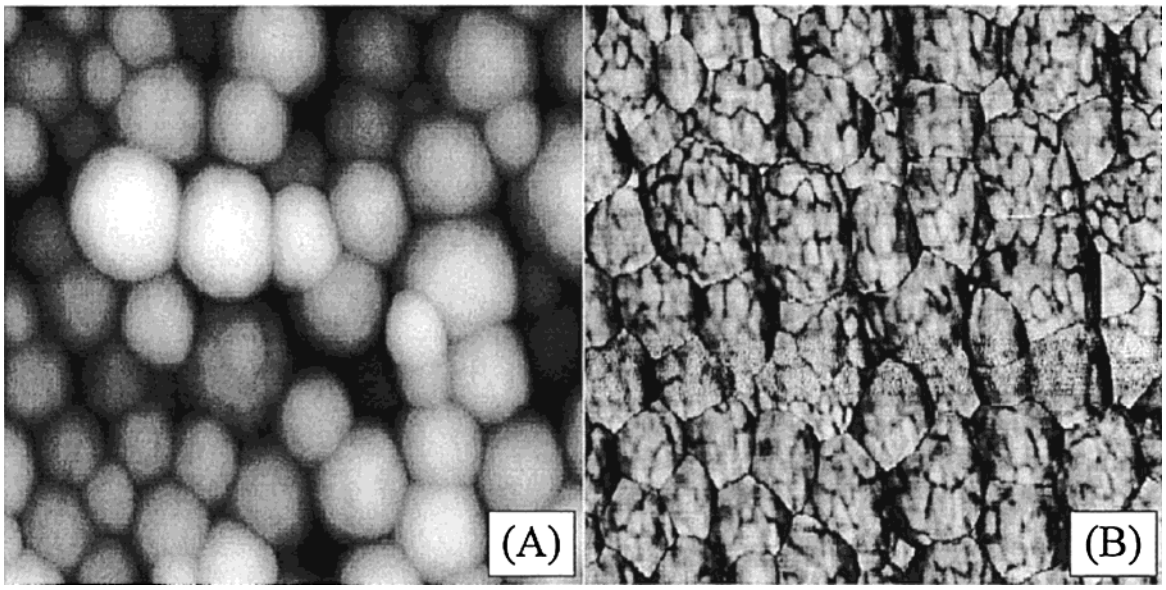

Figure 7. AFM height (A) and phase image (B) of pure core/shell latex **3** (DVB core/(BuA/FMA shell, 82/18 wt %)). The scan box is 1 μm × 1 μm. The height and phase scales are 0−125 nm and 0−30°, respectively, from dark to light color.

The ToF-SIMS spectra of pure latexes **2** (BuA/FMA, 98.6/1.4 wt %) and **4** (BuA/DVB core, 85/15 wt %)/(BuA/FMA shell, 92/8 wt %), along with their blends with latex **1** (BuA/S, 55/45 wt %), exhibit abundant evidence of fluorinated acetylide fragments at 293, 393, 493, ..., *m*/*z*. The spectrum of fluorinated core/shell latex **3** (DVB core/(BuA/FMA shell, 82/18 wt %) exhibited only weak ions attributable to acetylide fragments. Latex **3** (DVB core/(BuA/FMA shell, 82/18 wt %) does not form a film at room temperature, so the intact particle surface is being probed by ToF-SIMS. The spectrum was actually dominated by ions due to lauryl sulfate from the sodium salt used as a surfactant to stabilize the latex. The *n*-butyl acrylate present along with the fluorinated monomer in the shell also gave a weak fragment (71 *m*/*z*), suggesting that the poly(*n*-butyl acrylate-*co*-FMA) in the shell of this latex is present but not at the outer surface of the material in any large amount. All other spectra indicated a substantial fragment due to *n*-butyl acrylate at 71 *m*/*z*. In an effort to get semiquantitative information, the signal from the fluorinated acetylide fragment (293 *m*/*z*) was ratioed against the total ion yield, $I_{\text{acetylide}}/I_{\text{total}}$. This assumes that the total ion abundance is a reasonable common denominator and that sputtering yields are consistent between samples. The values of $I_{\text{acetylide}}/I_{\text{total}}$ for pure latexes **2** (BuA/FMA, 98.6/1.4 wt %) and **4** (BuA/DVB core, 85/15 wt %)/(BuA/FMA shell, 92/8 wt %) were 7.1×10^{-3} and 8.2×10^{-3}, respectively. The value of $I_{\text{acetylide}}/I_{\text{total}}$ for the fluorinated core/shell latex **3** (DVB core/(BuA/FMA shell, 82/18 wt %) was an order of magnitude smaller at 7.8×10^{-4} even though it contains ∼10−100 times more of the fluorinated monomer than the other two latexes. This is taken as evidence, albeit indirect, that FMA in the fluorinated core/shell latex **3** (DVB core/(BuA/FMA shell, 82/18 wt %) may have polymerized in the subsurface and is buried inside the core or at the interface between the core and shell. This would account for the low contact angles and atomic percentages of fluorine found with this sample. This could place some of the poly(divinylbenzene) from the core at the outer surface of the latex and would be expected and is observed to yield a mass spectrum that does not have abundant or useful fragment ions.

Atomic Force Microscopy Studies. In an attempt to gain additional information regarding surface composition and morphology, atomic force microscopy (AFM) was employed. The tapping mode technique (TMAFM) has proven to be a useful addition to the standard AFM arsenal in providing enhanced resolution through differences in mechanical properties of materials.[41,42] Tapping mode phase images have an analogy to viscoelastic measurements in rheological stress−strain measurements, although the comparison is not exact. The contrast in phase images results from a difference in phase of the oscillator drive and detector signals from the AFM cantilever. As a result, contrast enhancement is achieved using phase images to monitor stiffness variations in the sample relating to differences in Young's moduli in these areas. Interpretation of phase images acquired during tapping mode has been discussed at length in the literature.[43−46]

Shown in Figure 6 are the AFM height (A) and phase images (B) of the pure hydrocarbon latex **1** (BuA/S, 55/45 wt %). The images indicate that the latex **1** (BuA/S, 55/45 wt %) used as a matrix for the fluorinated latexes does not form a film at room temperature but yields discrete particles with particle diameters that are comparable to those measured by capillary hydrodynamic fractionation (412 nm). The narrow particle size distribution allows the particles to arrange in a hexagonally close-packed (hcp) array. The fluorinated latex **2** (BuA/FMA, 98.6/1.4 wt %) (not shown) is expected to form a film at room temperature with a $T_m \approx 11$ °C, and AFM images were featureless with the exception of small amounts of surfactant that appeared crystalline.

AFM height (A) and phase images (B) for the pure core/shell latex **3** (DVB core/(BuA/FMA shell, 82/18 wt %)) are shown in Figure 7. The images reflect well the particle size determined by capillary hydrodynamic fractionation of 213 nm. However, the breadth of the distribution (polydispersity index = 1.02) is sufficient to perturb the system from forming a hcp array. By virtue of the fact that discrete particles are observed in the AFM images indicates that this latex does not form a film at room temperature as confirmed by thermal analysis. The phase image (B) shown in Figure 7

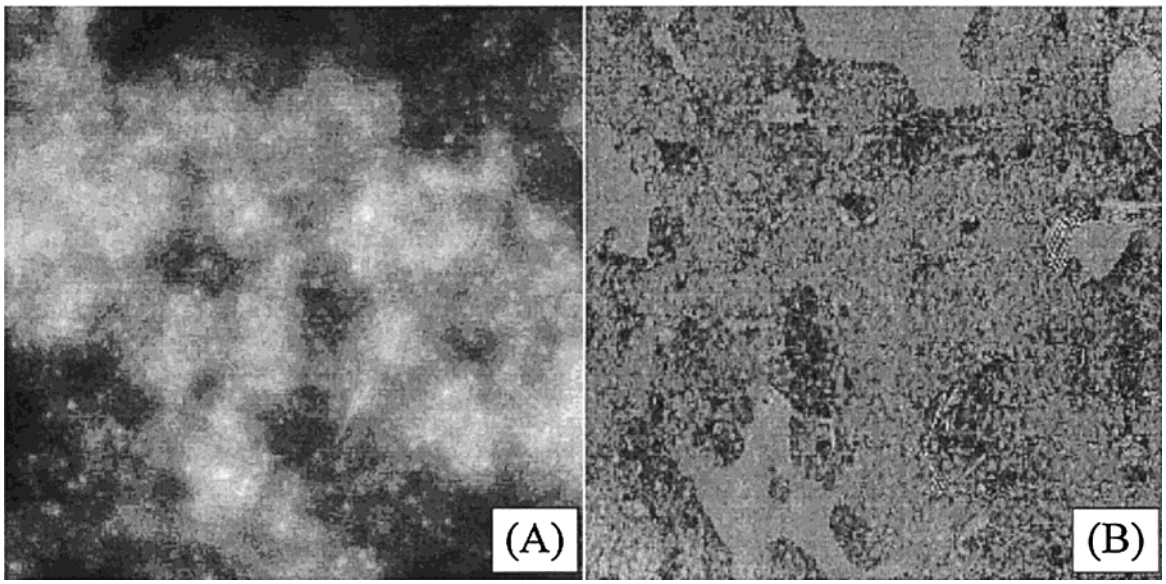

Figure 8. AFM height (left) and phase image (right) of pure core/shell latex **4** (DVB/BuA core, 15/85 wt %)/(BuA/FMA shell, 92/8 wt %). The scan box is 5 μm × 5 μm. The height and phase scales are 0−125 nm and 0−35°, respectively, from dark to light color.

demonstrates a "raspberry-like" morphology on each particle surface due to growth of the poly(*n*-butyl acrylate-*co*-FMA) shell or partial shell on the poly(divinylbenzene) core. This type of morphology has been observed previously during preparation of other latex systems[47−49] and is thought to be due to kinetic control of the second stage when the polymerization rate exceeds that of phase separation. Particle morphology in core/shell latexes is largely a result of interfacial tensions of the respective components against each other and the continuous phase.[47] Latex **3** (DVB core/(BuA/FMA shell, 82/18 wt %)) contains more of the fluorinated monomer in its shell than latex **4** (BuA/DVB shell, 85/15 wt %)/(BuA/FMA shell, 92/8 wt %). As a consequence, the shell interfacial tension against water should be larger and may favor placing the fluorinated portion of the copolymer toward the inside (seed) of the composite latex. Contact angle goniometry, XPS, and ToF-SIMS do not indicate much fluorine in the outermost portion of the latex particle.

AFM topography (A) and phase images (B) for the pure core/shell latex **4** (BuA/DVB shell, 85/15 wt %)/(BuA/FMA shell, 92/8 wt %) are shown in Figure 8. The height image appears to be intermediate (partial coalescence or sintering) in morphology between the pure latex **2** (BuA/FMA, 98.6/1.4 wt %) and pure core/shell latex **3** (DVB core/(BuA/FMA shell, 82/18 wt %)). The image suggests the presence of particles that are in some stage of sintering. Because of the relationship between sintering rate, r, and capillary number, C_a ($r \propto 1/C_a \propto \gamma/\eta$ where η is viscosity and γ is interfacial tension between latex particles),[50] the fluorine-containing latexes should all be sluggish film-formers compared to hydrocarbon analogues of comparable molecular weight.

The real value of the TMAFM phase imaging technique is exemplified by examination of blends of fluorinated and hydrocarbon acrylic copolymer latexes. AFM height (A) and phase images (B) for a blend of hydrocarbon latex **1** (BuA/S, 55/45 wt %) with two different levels of fluorinated latex **2** (BuA/FMA, 98.6/1.4 wt %) are shown in Figures 9 and 10, for a mole fraction (χ_{FMA}) of FMA in the films of 5.1×10^{-4} and 2.6×10^{-3}, respectively. This corresponds to volume fractions of fluorinated latex $V_f \approx 3.7 \times 10^{-2}$ and 1.86×10^{-1}, respectively. While the hcp array of the larger particle size latex **1** (BuA/S, 55/45 wt %) is visible clearly at low FMA mole fraction (Figure 9) and less so at the higher FMA mole fraction (Figure 10), the surfaces are covered by a thin (≈50−70 Å) layer of material that is thought to contain fluorinated copolymer.

The height image shown in Figure 9 shows clearly two separate phases as expected from a blend of incompatible latexes **1** (BuA/S, 55/45 wt %) and **2** (BuA/FMA, 98.6/1.4 wt %). The large, non-film-forming hydrocarbon latex is evident in many regions in a hexagonally close-packed aray. This is true especially in the low-lying regions in the height image. If the height image is overlaid on the phase image (Figure 9B), the low-lying regions correspond to the higher (lighter colored) phase (∼30°), thought to be non-film-forming hydrocarbon latex **1** (BuA/S, 55/45 wt %). If the height image is again overlaid on the phase image, the elevated regions containing a film of fluorinated latex **2** correspond directly to the darker, lower phase image under present experimental conditions. The results from contact angle goniometry (Figure 3), XPS (Table 2), and ToF-SIMS discussed earlier support the conclusion that the blend film is covered substantially by fluorinated latex **2** (BuA/FMA, 98.6/1.4 wt %). On the basis of material properties of film forming fluorinated latex **2** and non-film-forming hydrocarbon latex **1**, the dark phase can be assigned tentatively to a "softer" region of fluorinated material.

Since a complete frequency-sweep TMAFM experiment [51] as a function of drive amplitude A_0, set-point amplitude A_{sp}, and set-point ratio r_{sp} ($=A_{sp}/A_0$) was not conducted, an assignment of the two phases is equivocal. Numerous studies have shown disagreement between assignment of phase shifts to hard/soft polymeric blends due to the fact that relative contrast in phase images results from a choice of instrumental parameters such as A_0 and r_{sp}.[41,44,52,53] In a number of studies, it was demonstrated that height and phase images can be reversed by changing instrumental parameters.[41,42,52] The reverse in contrast is thought to be due to changes in tip−sample interactions when crossing the attractive−repulsive force regime by changing parameters

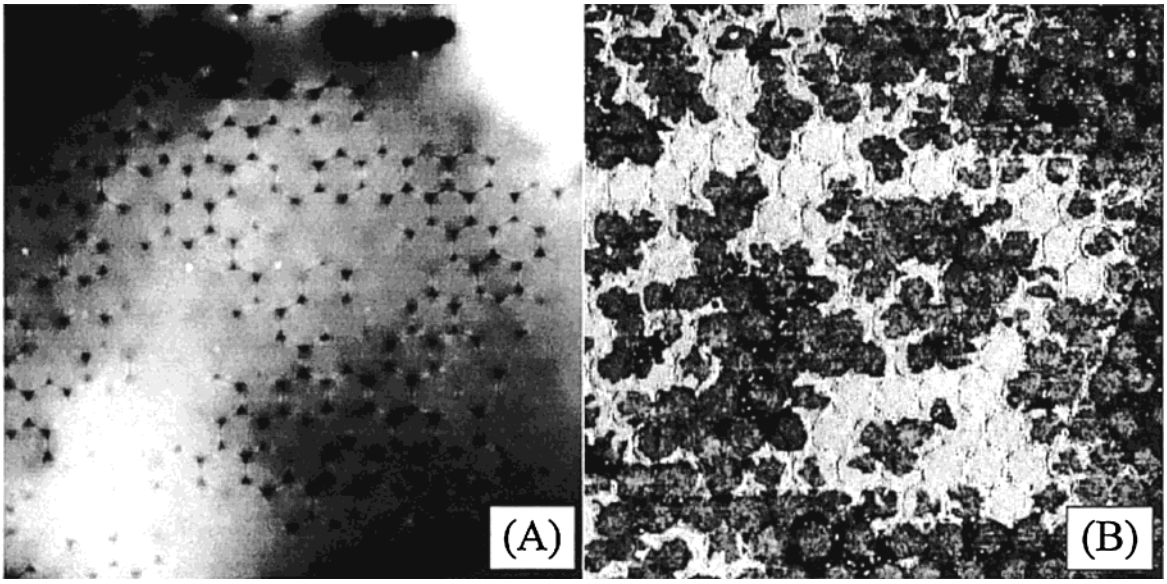

Figure 9. AFM height (A) and phase image (B) of a blend of hydrocarbon latex **1** (BuA/S, 55/45 wt %) and fluorinated latex **2** (BuA/FMA, 98.6/1.4 wt %) with mole fraction of FMA $\approx 5.1 \times 10^{-4}$ and fluorinated latex volume fraction $\approx 3.7 \times 10^{-2}$. The scan box is 5 μm × 5 μm. The height and phase scales are 0−50 nm and 0−30°, respectively, from dark to light color.

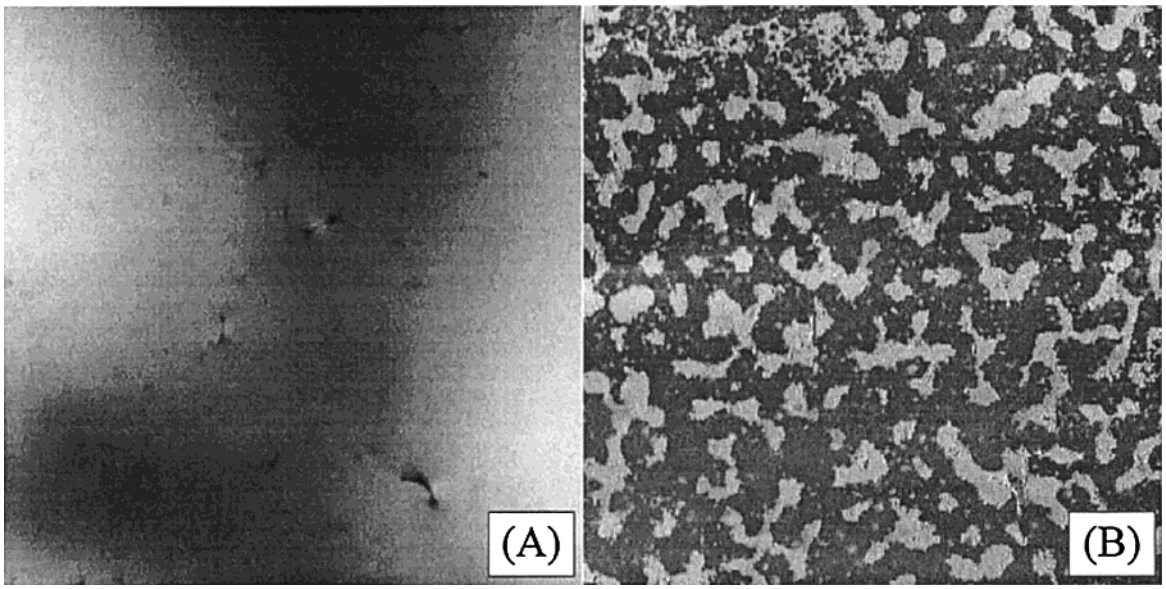

Figure 10. AFM height (A) and phase image (B) of a blend of hydrocarbon latex **1** (BuA/S, 55/45 wt %) and fluorinated latex **2** (BuA/FMA, 98.6/1.4 wt %) with mole fraction of FMA $= 2.6 \times 10^{-3}$ and fluorinated latex volume fraction ≈ 0.19. The scan box is 5 μm × 5 μm. The height and phase scales are 0−70 nm and 0−30°, respectively, from dark to light color.

such as tip shape, cantilever force constant, A_0, and r_{sp}.[51] To examine the effect of instrumental parameters on observed height and phase images, a set of experiments was performed on a blend of latex **1** (BuA/S, 55/45 wt %) and **2** (BuA/FMA, 98.6/1.4 wt %) with $\chi_{FMA} \approx 5.1 \times 10^{-4}$ by varying r_{sp}. The TMAFM images are shown in Figure 11. There is no height or phase reversal as the set-point amplitude is increased from ~0.76 to ~1.2 V with a concomitant decrease in tapping force; however, there is a noticeable increase in contrast of both height and phase at lower A_{sp}. The increased contrast is suggestive that the phase difference observed is due to local sample stiffness under the present experimental conditions. The topography of the sample was such that lateral force imaging, unfortunately, could not be used to aid in phase identification. Furthermore, topography of the sample brings about the added complication that the effect of the mutual radius of curvature[45] of the sample and tip needs to be factored into the phase image analysis.

There is another feature evident in the height image shown in Figure 9A that may lend some insight into the mechanism responsible for the large surface excess observed with a blend of latexes **1** and **2**. The coalesced fluorinated latex **2** (BuA/FMA, 98.6/1.4 wt %) has phase separated *completely* from hydrocarbon latex **1** (BuA/S, 55/45 wt %). There are not many examples of this type of system in the literature, but this is different than has been observed previously with asymmetric latex blends where a composite surface was found.[8] The connectivity of the fluorinated phase shown in Figures 9 and 10 is reminiscent of a percolated network confined to two dimensions at a surface. Percolation effects have been observed previously in the bulk of latex blends by small-angle neutron scattering.[14] The hydrocarbon latex **1** (BuA/S, 55/45 wt %) is organized into a crystalline-like

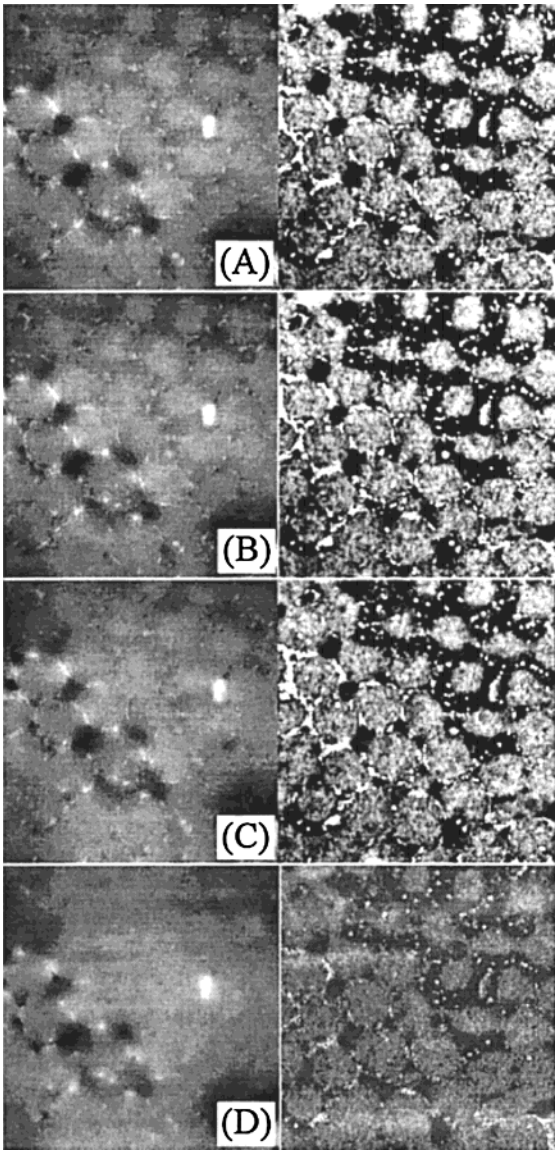

Figure 11. AFM height (left) and phase images (right) of a blend of hydrocarbon latex **1** (BuA/S, 55/45 wt %) and fluorinated latex **2** (BuA/FMA, 98.6/1.4 wt %) with mole fraction of FMA = 5.1×10^{-4} and fluorinated latex volume fraction $\approx 3.7 \times 10^{-2}$ as a function of set-point amplitude voltage. Images A, B, C, and D correspond to set points of 0.7626, 1.002, 1.088, and 1.263 V, respectively, and decreasing tapping force. The scan box is 2 μm × 2 μm. The height and phase scales are 0−25 nm and 0−25°, respectively, from dark to light color.

hcp array on the substrate. While the pure hydrocarbon latex **1** forms a routine hcp array on the substrate alone (see Figure 6, for example), the blend with fluorinated latex **2** shows what appears to be a *more* ordered crystalline-like hcp array on the substrate. Phase separation must have occurred in solution prior to coalescence of the fluorinated latex **2** (BuA/FMA, 98.6/1.4 wt %) since pure fluorinated latex **2** does not coagulate or phase separate in a mixture with hydrocarbon latex **1** in solution. It is also doubtful that phase separation of the two latexes could have taken place after the film dried as the hcp array of hydrocarbon latex **1** is ordered too well to have formed in the solid state. Theoretical work by Biben and Hansen has shown that phase separation is possible from dense binary mixtures of hard spheres when the size ratio (small particle/large particle) is <0.2 at comparable packing fractions.[20] In the present case, the size ratio for the blend of latexes **1** and **2** is ≈0.16, making phase separation of the latex mixture possible theoretically. On the basis of morphology and transparency studies on asymmetric latex blends, Winnik et al. have presented evidence for phase separation when the particle size ratio decreases below a critical threshold.[54] However, when the particle size ratio is close to unity, electrostatic effects can dominate as shown in a study of conductive composite films prepared from aqueous colloidal dispersions.[55] In addition, work by Dinsmore and Yodh has shown that large particles can be confined entropically and preferentially to a substrate from an asymmetric blend of hard spheres (polystyrene) due to excluded-volume effects.[56] From conductometric measurements on solutions of latexes used in the present study, a Debye screening length for the particles can be estimated in a range ≈10−30 nm that is much smaller than particle diameters and, therefore, qualifies these particles as "hard" spheres. Such a mechanism may be contributing to phase separation observed in the current study by pinning the large particle size latex to the substrate surface. It is doubtful that electrostatic effects are responsible for preferential confinement of latex **1** (BuA/S, 55/45 wt %) or, conversely, exclusion of latex **2** (BuA/FMA, 98.6/1.4 wt %) from the substrate. Both small and large particle latexes were prepared using anionic surfactants, resulting in negative ζ potentials, and the substrates used in the current study would have a net anionic charge under film preparation conditions.

The phase image of the mixture with $\chi_{FMA} \approx 2.6 \times 10^{-3}$, shown in Figure 10, is similar to that of Figure 9, except that it appears that a larger area fraction of the hydrocarbon latex **1** (BuA/S, 55/45 wt %) is covered by the fluorinated material from latex **2** (BuA/FMA, 98.6/1.4 wt %). This finding agrees well with the conclusion that ∼80% of the surface is covered with low free energy material as estimated by eq 2 using contact angle data and XPS which shows the surface to be dominated by material from the fluorinated latex **2** (BuA/FMA, 98.6/1.4 wt %).

A mixture of hydrocarbon latex **1** (BuA/S, 55/45 wt %) and fluorinated core/shell latex **3** (DVB core/(BuA/FMA shell, 82/18 wt %)) with $\chi_{FMA} \approx 3.1 \times 10^{-2}$ and 1.3×10^{-1} ($V_f \approx 4.1 \times 10^{-2}$ and 1.9×10^{-1}, respectively) was examined by AFM, and the height (A) and phase images (B) are shown in Figures 12 and 13, respectively. The hexagonally close-packed array of hydrocarbon latex **1** (BuA/S, 55/45 wt %) is still visible with no evidence of coverage by fluorinated material with the low χ_{FMA} images exhibited in Figure 12. The phase image reflects the height image well. The height and phase images in Figure 13 with $\chi_{FMA} \approx 1.3 \times 10^{-1}$ exhibit a disrupted array of large hydrocarbon latex **1** (BuA/S, 55/45 wt %) particles interspersed with smaller particles of fluorinated core/shell latex **3** (DVB core/(BuA/FMA shell, 82/18 wt %)). There is little contrast enhancement in the phase image between fluorocarbon and hydrocarbon phases. Compare these images to those shown in Figures 6 and 7 for the pure materials. This should not be surprising since the two latexes do not form films at room temperature and are both relatively "stiff". It is difficult to estimate a surface coverage of fluorinated material from the images shown in Figures 12 and 13; however, contact angle goniometry, XPS, and

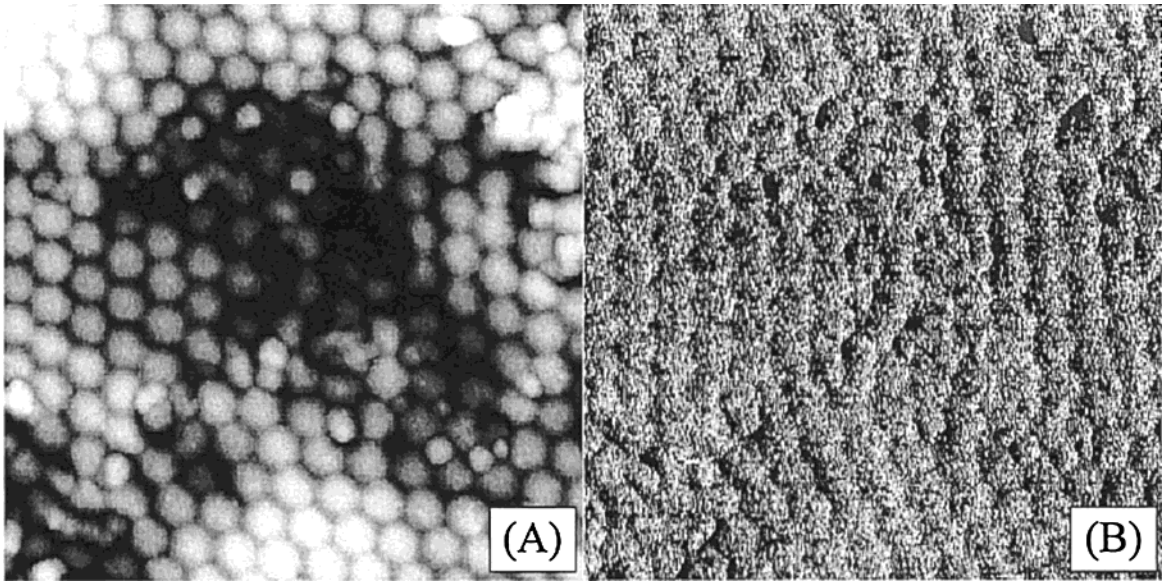

Figure 12. AFM height (left) and phase image (right) of a blend of hydrocarbon latex **1** (BuA/S, 55/45 wt %) and fluorinated core/shell latex **3** (DVB core/(BuA/FMA shell, 82/18 wt %)) with mole fraction of FMA $\approx 3.1 \times 10^{-2}$ and fluorinated latex volume fraction $\approx 4.1 \times 10^{-2}$. The scan box is 5 μm $\times$ 5 μm. The height and phase scales are 0−150 nm and 0−30°, respectively, from dark to light color.

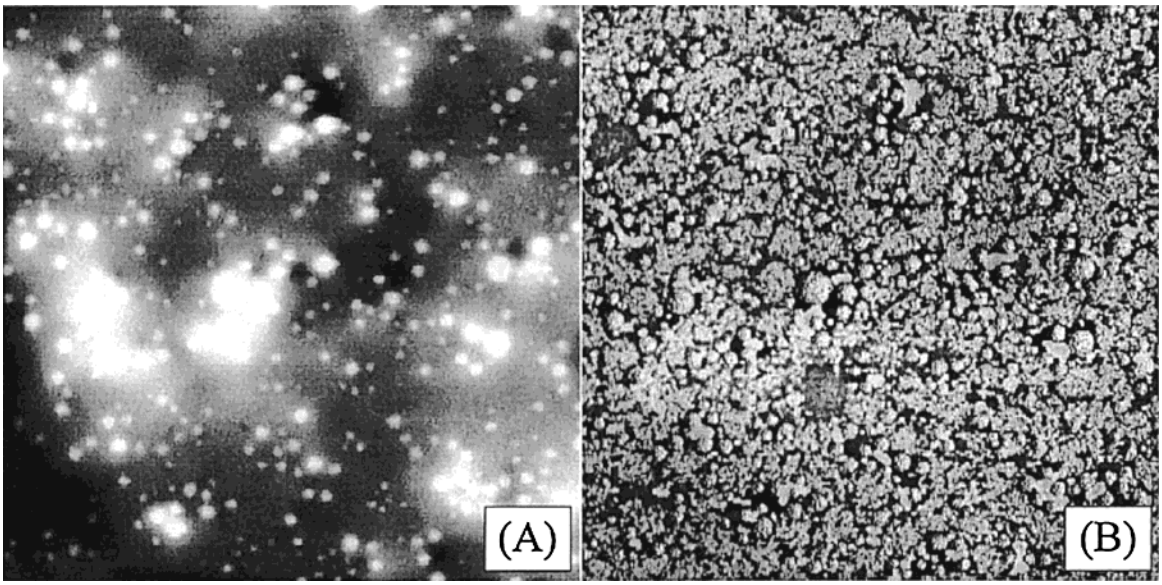

Figure 13. AFM height (A) and phase image (B) of a blend of hydrocarbon latex **1** (BuA/S, 55/45 wt %) and fluorinated core/shell latex **3** (DVB core/(BuA/FMA shell, 82/18 wt %)) with mole fraction of FMA $\approx 1.3 \times 10^{-1}$ and fluorinated latex volume fraction ≈ 0.19. The scan box is 5 μm $\times$ 5 μm. The height and phase scales are 0−75 nm and 0−30°, respectively, from dark to light color.

ToF-SIMS show little fluorinated material in excess at the surface. The contact angle data shown in Figure 5 indicate that pure core/shell latex **3** (DVB core/(BuA/FMA shell, 82/18 wt %)) has a surface containing little low free energy fluorinated copolymer.

Atomic force microscopy was next used to examine a film prepared from a blend of the hydrocarbon latex **1** (BuA/S, 55/45 wt %) with the fluorinated core/shell latex **4** (BuA/DVB core, 85/15 wt %)/(BuA/FMA shell, 92/8 wt %) at $\chi_{FMA} \approx 8.5 \times 10^{-3}$ and 4.2×10^{-2} ($V_f \approx 4.1 \times 10^{-2}$ and 3.85×10^{-1}, respectively) with the height (A) and phase images (B) shown in Figures 14 and 15, respectively. At $\chi_{FMA} \approx 8.5 \times 10^{-3}$, the height image shows the hydrocarbon latex **1** (BuA/S, 55/45 wt %) which is discernible below a layer of, what is thought to be, fluorinated material. The height image in Figure 14 also shows some discrete particles (light colored) of the fluorinated core/shell latex **4** ((BuA/DVB core, 85/15 wt %)/(BuA/FMA shell, 92/8 wt %)) that have not yet sintered and are interspersed between the large particles of latex **1** (BuA/S, 55/45 wt %). The phase image in Figure 14 does not exhibit any of the underlying hydrocarbon latex, but small particles of the fluorinated core/shell latex **4** ((BuA/DVB core, 85/15 wt %)/(BuA/FMA shell, 92/8 wt %)) are visible. There is an unusual feature exhibited by this mixture in the presence of "tracks" of high phase (light colored), relatively stiff material of unknown origin associated with the larger underlying hydrocarbon latex **1** (BuA/S, 55/45 wt %) particles. These features do not appear in the phase image of the pure core/shell latex **4** (BuA/DVB core, 85/15 wt %)/(BuA/FMA shell, 92/8 wt %) or in the pure hydrocarbon latex **1** (BuA/S, 55/45 wt %). The "tracks" also do not appear attributable to the presence of aggregated surfactant as the same surfactant system is used consistently throughout and are not visible on

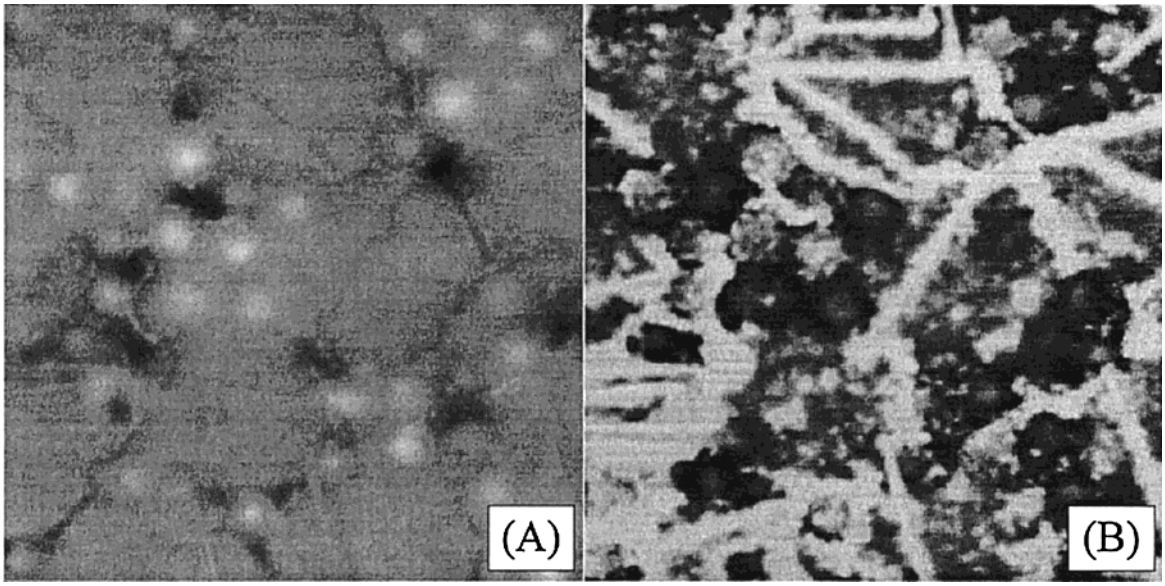

Figure 14. AFM height (A and C) and phase image (B) of a blend of hydrocarbon latex **1** (BuA/S, 55/45 wt %) and fluorinated core/shell latex **4** ((BuA/DVB core, 85/15 wt %)/(BuA/FMA shell, 92/8 wt %)) with mole fraction of FMA $\approx 8.5 \times 10^{-3}$ and fluorinated latex volume fraction $\approx 4.1 \times 10^{-2}$. The scan box is 1 μm × 1 μm. The height and phase scales are 0−25 nm and 0−45°, respectively, from dark to light color.

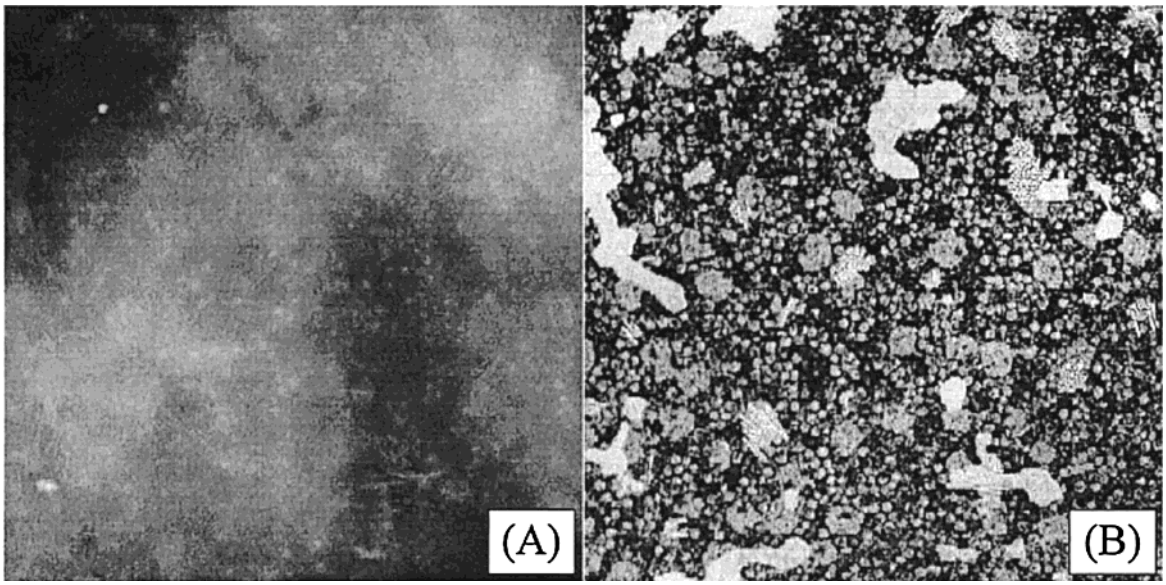

Figure 15. AFM height (A) and phase image (B) of a blend of hydrocarbon latex **1** (BuA/S, 55/45 wt %) and fluorinated core/shell latex **4** ((BuA/DVB core, 85/15 wt %)/(BuA/FMA shell, 92/8 wt %)) with mole fraction of FMA $= 4.2 \times 10^{-2}$ and fluorinated latex volume fraction ≈ 0.38. The scan box is 5 μm × 5 μm. The height and phase scales are 0−75 nm and 0−60°, respectively, from dark to light color.

samples with larger mole fractions of copolymerized FMA. The height image shown Figure 15 with $\chi_{FMA} \approx 4.2 \times 10^{-2}$ demonstrates the surface to be nearly covered by a thick layer of fluorochemical. The phase image shows lighter colored (stiffer) regions whose particle size diameter matches that of the hydrocarbon latex **1** (BuA/S, 55/45 wt %) surrounded by a large number of smaller particles of fluorinated core/shell latex **4** (BuA/DVB core, 85/15 wt %)/(BuA/FMA shell, 92/8 wt %).

Percolation and Excluded-Volume Effects. With the exception of the blend of latex **1** (BuA/S, 55/45 wt %) and the fluorinated core/shell latex **3** (DVB core/(BuA/FMA shell, 82/18 wt %)), all of the asymmetric mixtures showed a remarkable surface excess of fluorinated copolymer well above bulk levels as detected by contact angle goniometry and XPS. The relatively poor performance of the hydrocarbon latex **1** (BuA/S, 55/45 wt %) and fluorinated core/shell latex **3** (DVB core/(BuA/FMA shell, 82/18 wt %)) blend in supplying surface active fluorinated copolymer can be attributed to the behavior of pure fluorinated core/shell latex as discussed earlier. The densities of all the fluorinated latexes were comparable to or greater than the hydrocarbon latex, so gravitational effects cannot account for the remarkable excess of fluorinated copolymer observed in many cases.

Unfortunately, the experimental design did not include adequate tests to discriminate unequivocally between percolation and excluded-volume effects in causing a substantial gradient of fluorinated, low surface free energy material to be in excess at the film surface. However, the arguments of percolation theory can be combined with contact angle data in an effort to grasp its magnitude and, perhaps, separate its contri-

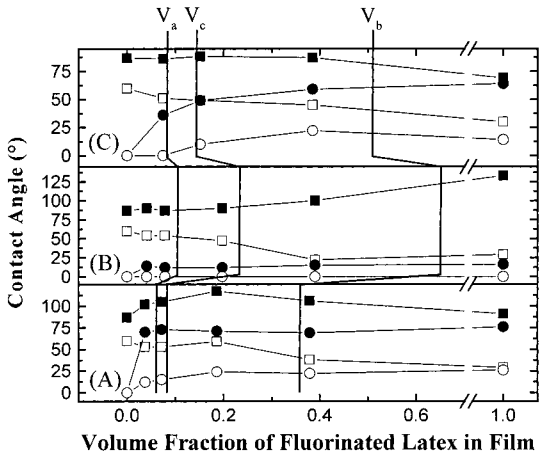

Figure 16. Contact angle data and percolation threshold values for asymmetric blends of the hydrocarbon latex **1** (BuA/S, 55/45 wt %) with (A) latex **2** (BuA/FMA, 98.6/1.4 wt %), (B) latex **3** (DVB core/(BuA/FMA shell, 82/18 wt %)) and (C) latex **4** ((BuA/DVB core, 85/15 wt %)/(BuA/FMA shell, 92/8 wt %)). A volume fraction of 0 corresponds to the pure hydrocarbon latex **1** (BuA/S, 55/45 wt %), while a volume fraction of 1 indicates pure fluorinated latex. Shown are water advancing (■) and receding (□) and hexadecane advancing (●) and receding (○) contact angle values.

bution to the observed results from excluded-volume effects.

On the basis of geometric considerations in asymmetric mixtures of hard spheres, equations have been derived to define various stages in percolation:[10,11] (i) V_a is the volume fraction at which the small particle size material begins to form infinitely long chains, (ii) V_b is the volume fraction at which small particle size material fills all planar lattice sites, and (iii) V_c is the critical volume fraction of small particle size material that indicates a transition from 1- or 2-D infinite chains to 3-D coverage of the large particles by the smaller ones with $V_a < V_c < V_b$.

If the assumption can be made that complete coverage of a film by the fluorinated copolymer component leads to the highest possible contact angles (eq 2), then data can be examined in light of the definitions, especially V_b, used to define critical stages in percolation. Shown in Figure 16 are plots of contact angle data obtained on asymmetric blends of the hydrocarbon latex **1** (BuA/S, 55/45 wt %) with latexes **2** (BuA/FMA, 98.6/1.4 wt %), **3** (DVB core/(BuA/FMA shell, 82/18 wt %)), and **4** ((BuA/DVB core, 85/15 wt %)/(BuA/FMA shell, 92/8 wt %)) as a function of volume fraction of fluorinated small particle size latex. Percolation thresholds at V_a, V_b, and V_c are shown as solid vertical lines on the plots. Threshold values were calculated, faute de mieux, for a hexagonal lattice with a coordination number of 6.

For the asymmetric blend of hydrocarbon latex **1** (BuA/S, 55/45 wt %) with the fluorinated latexes **2** (BuA/FMA, 98.6/1.4 wt %) and **4** (BuA/DVB shell, 85/15 wt %)/(BuA/FMA shell, 92/8 wt %), the contact angles appear to reach relative maxima well before the threshold for filling of all planar lattice sites (in essence, surface saturation), V_b, is reached. In fact, the contact angles appear to have maximized between V_a and V_c, and contact angle values in this region are actually *higher* than films prepared from the pure fluorinated acrylic copolymer latexes. The lower contact angles obtained on films of pure fluorinated latexes can be explained by a larger concentration of relatively high surface free energy surfactant as compared to blends with the larger poly(*n*-butyl acrylate-*co*-styrene) latex. The relatively smaller, higher surface area-to-volume ratio, fluorinated acrylic copolymer latexes require a higher concentration of surfactant for stability than larger sized latexes.

Evidence supporting excluded-volume effects on aggregation is shown in Figures 9, 10, and 16A for the blend of latex **1** (BuA/S, 55/45 wt %) and **2** (BuA/FMA, 98.6/1.4 wt %). Hexadecane contact angles reach a maximum between V_a and V_c, while AFM images demonstrate complete phase separation of the two components.

Further substantiation of excluded-volume effects is offered by examination of Figures 14 and 15. For $\chi_{FMA} \approx 8.5 \times 10^{-3}$ and 4.2×10^{-2}, both phase images indicate clearly a large excess of the smaller particle fluorinated latex **4** (BuA/DVB core, 85/15 wt %)/(BuA/FMA shell, 92/8 wt %) at or near the surface. These values of χ_{FMA} correspond to volume fractions ≈0.08 and 0.39, respectively, and are both lower than $V_b \approx 0.52$ calculated for this asymmetric mixture. In fact, the volume fraction of 0.08 is much closer to V_a than V_b. Considering that percolation theory predicts formation of incipient infinite chains of the smaller size component at V_a, the observation of surface saturation (Figure 16C) by the fluorinated latex at a volume fraction of 8×10^{-2} may indicate the importance of excluded-volume effects in promoting aggregation of the smaller component in an asymmetric mixture. In addition, the values of χ_{FMA} are less than the void volume, V_v, of close-packed spheres ($V_v = 0.26$ for face-centered cubic; =0.34 random).[54] A complete evaluation of percolation and excluded-volume effects awaits further study.

Conclusions

Latexes, of a variety of morphologies, containing fluorinated copolymers have been prepared easily using emulsion and miniemulsion polymerization techniques. By controlling preparation conditions carefully, a variety of relatively narrow particle size distributions were obtained. In addition, a hydrocarbon acrylic copolymer latex, poly(*n*-butyl acrylate-*co*-styrene), was prepared as a host matrix to be used in blends. Latexes were characterized by thermal and elemental analysis and for particle size and molecular weight.

Preparation of a latex containing poly(*n*-butyl acrylate-*co*-FMA), **2**, and two core/shell latexes **3** (DVB core/(BuA/FMA shell, 82/18 wt %) and **4** (BuA/DVB core, 85/15 wt %)/(BuA/FMA shell, 92/8 wt %) allowed for the study of formation of low free energy surfaces using particles of three different morphologies. Latex **1** is of homogeneous morphology, while latexes **3** and **4** were of the core/shell variety containing a highly cross-linked and a partially cross-linked core, respectively. Because of monomers chosen and particle morphology, each latex has a different propensity to form films and low free energy surfaces.

By using a blend of latex particles consisting of a large particle size poly(*n*-butyl acrylate-*co*-styrene) latex with a small particle size, incompatible, fluorine-containing acrylic latex, percolation and perhaps excluded volume can be exploited in allowing the fluorinated component of the blend to be in excess at the surface. These phenomena can be used either independently or synergistically to allow small fluorinated latex particles to aggregate near a surface. In addition, both phenomena are more pronounced with increasing particle size

disparity. In addition, favorable thermal properties, such as T_g or T_m near room temperature, can allow fluorinated material to spread across the film surface, reducing further surface free energy according to eq 2 by increasing coverage. Films prepared from blends of hydrocarbon and fluorinated acrylic copoymer latexes, as well as pure latexes, were examined by contact angle goniometry, XPS, ToF-SIMS, and AFM.

Tapping mode AFM was employed successfully to record height and phase images on blends of latexes as well as the pure component latexes. The phase images are capable of differentiating the fluorinated acrylic copolymer component from the hydrocarbon acrylic copolymer matrix on the basis of mechanical property differences. The phase and height AFM images are corroborated well by contact angle goniometry, XPS, and ToF-SIMS. The estimates of surface coverage, using contact angle data and eq 2, by fluorinated material in films prepared from blends agree reasonably well with AFM images. Relatively thick (∼100 Å) films of fluorinated copolymer are observed on films providing low free energy surfaces.

Evidence is given that the phenomena of percolation and excluded volume may be used to deliver fluorinated, low free energy material to the surface of an asymmetric mixture with disparate particle sizes. Larger surface excesses of fluorinated, low free energy material are observed as the particle size disparity increases. The surface excess of fluorinated material and decrease in surface free energy tracks the increase in particle size ratio for these mixtures when compared on an equal mole fraction basis of fluorine in the mixture. While it is difficult to discern between the effects of percolation and excluded volume, mixtures of latex **1** (BuA/S, 55/45 wt %) with fluorinated latexes **2** (BuA/FMA, 98.6/1.4 wt %) and **4** (BuA/DVB shell, 85/15 wt %)/(BuA/FMA shell, 92/8 wt %) exhibit relative contact angle maxima (surface free energy minima) well below the volume fraction predicted by percolation theory for filling of all planar lattice sites. This may indicate that excluded-volume effects play a synergistic role in allowing fluorinated material to be in excess at the film surface.

Acknowledgment. The authors thank Nancy G. Tassi for the AFM data and help with its interpretation.

References and Notes

(1) Adamson, A. W. *Physical Chemistry of Surfaces*, 5th ed.; Wiley: New York, 1990; Chapter X.
(2) Wu, S. *Polymer Interface and Adhesion*; Marcell Dekker: New York, 1982; Chapter 3.
(3) Johnson, R. E., Jr.; Dettre, R. H. In *Wettability*; Berg, J. C., Ed.; Marcel Dekker: New York, 1993; Chapter 1.
(4) Hoernschemeyer, D. *J. Phys. Chem.* **1966**, *70*, 2628.
(5) Marion, P.; Beinert, G.; Juhué, D.; Lang, J. *Macromolecules* **1997**, *30*, 123.
(6) Marion, P.; Beinert, G.; Juhué, D.; Lang, J. *J. Appl. Polym. Sci.* **1997**, *64*, 2409.
(7) Linemann, R. F.; Malner, T. E.; Brandsch, R.; Bar, G.; Ritter, W.; Muelhaupt, R. *Macromolecules* **1999**, *32*, 1715.
(8) Eckersley, S. T.; Helmer, B. J. *J. Coat. Technol.* **1997**, *69*, 97.
(9) Sahimi, M. *Applications of Percolation Theory*; Taylor and Francis: London, 1994; Chapter 2.
(10) Kusy, R. P. *J. Appl. Phys.* **1977**, *48*, 5301.
(11) Malliaris, A.; Turner, D. T. *J. Appl. Phys.* **1971**, *42*, 614.
(12) Banerjee, P.; Mandal, B. M. *Macromolecules* **1995**, *28*, 3940.
(13) Banerjee, P. *Eur. Polym. J.* **1998**, *34*, 841.
(14) Chevalier, Y.; Hidalgo, M.; Cavaillé, J. Y.; Cabane, B. *Prog. Org. Coat.* **1997**, *32*, 35.
(15) Cooper, E. C.; Vincent, B. *J. Phys. D: Appl. Phys.* **1989**, *22*, 1580.
(16) Favier, V.; Chanzy, H.; Cavaillé, J. Y. *Macromolecules* **1995**, *28*, 6365.
(17) Matsumoto, M.; Ichino, T.; Rutt, J. S.; Nishi, S. *J. Polym. Sci., Part A: Polym. Chem.* **1994**, *32*, 2551.
(18) Oosawa, F.; Asakura, S. *J. Chem. Phys.* **1954**, *22*, 1255.
(19) Vrij, A. *Pure Appl. Chem.* **1976**, *48*, 471.
(20) Biben, T.; Hansen, J.-P. *Phys. Rev. Lett.* **1991**, *66*, 2215.
(21) Bartlett, P.; Ottewill, R. H. *Langmuir* **1992**, *8*, 1919.
(22) Sweetser, P. B. *Anal. Chem.* **1956**, *28*, 1766.
(23) Wickbold, R. *Angew. Chem.* **1952**, *64*, 133.
(24) Tanaka, T.; Fujimoto, T.; Shibayama, K. *J. Appl. Polym. Sci.* **1979**, *23*, 1131.
(25) Vijayendran, B. R.; Bone, T.; Sawyer, L. C. *J. Disp. Sci. Technol.* **1982**, *3*, 81.
(26) Thomas, R. R.; Stephans, L. E., unpublished results.
(27) Fox, T. G.; Flory, P. J. *J. Appl. Phys.* **1950**, *21*, 581.
(28) Fox, T. G. *Bull. Am. Phys. Soc.* **1956**, *2*, 123.
(29) Schönherr, H.; Ringsdorf, H.; Jaschke, M.; Butt, H.-J.; Bamburg, E.; Allinson, H.; Evans, S. D. *Langmuir* **1996**, *12*, 3898.
(30) Schönherr, H.; Ringsdorf, H. *Langmuir* **1996**, *12*, 3891.
(31) Cassie, A. B. D. *Discuss. Faraday Soc.* **1948**, *3*, 11.
(32) Dettre, R. H.; Johnson, R. E., Jr. *J. Phys. Chem.* **1965**, *69*, 1507.
(33) Johnson, R. E., Jr.; Dettre, R. H. *J. Phys. Chem.* **1964**, *68*, 1744.
(34) Neumann, A. W.; Good, R. J. *J. Colloid Interface Sci.* **1972**, *38*, 341.
(35) Schwartz, L. W.; Garoff, S. *Langmuir* **1985**, *1*, 220.
(36) Schwartz, L. W.; Garoff, S. *J. Colloid Interface Sci.* **1985**, *106*, 422.
(37) Wenzel, R. N. *Ind. Eng. Chem.* **1936**, *28*, 988.
(38) Wenzel, R. N. *J. Phys. Colloid Chem.* **1949**, *53*, 1466.
(39) Swain, P. S.; Lipowsky, R. *Langmuir* **1998**, *14*, 6772.
(40) Thomas, R. R.; Anton, D. R.; Graham, W. F.; Darmon, M. J.; Sauer, B. B.; Stika, K. M.; Swartzfager, D. G. *Macromolecules* **1997**, *30*, 2883.
(41) McLean, R. S.; Sauer, B. B. *Macromolecules* **1997**, *30*, 8314.
(42) Sauer, B. B.; McLean, R. S.; Thomas, R. R. *Langmuir* **1998**, *14*, 3045.
(43) Brandsch, R.; Bar, G.; Whangbo, M. H. *Langmuir* **1997**, *13*, 6349.
(44) Magonov, S. N.; Elings, V.; Whangbo, M. H. *Surf. Sci.* **1997**, *375*, L385.
(45) Behrend, O. P.; Odoni, L.; Loubet, J. L.; Burnham, N. A. *Appl. Phys. Lett.* **1999**, *75*, 2551.
(46) Bar, G.; Delineau, L.; Brandsch, R.; Bruch, M.; Whangbo, M.-H. *Appl. Phys. Lett.* **1999**, *75*, 4198.
(47) Chen, Y.-C.; Dimonie, V.; El-Aasser, M. S. *J. Appl. Polym. Sci.* **1991**, *42*, 1049.
(48) Winnik, M. A.; Zhao, C. L.; Shaffer, O.; Shivers, R. R. *Langmuir* **1993**, *9*, 2053.
(49) Durant, Y. G.; Sundberg, C. *J. Appl. Polym. Sci.* **1995**, *58*, 1607.
(50) Schonhorn, H.; Frisch, H. L.; Kwei, T. K. *J. Appl. Phys.* **1966**, *37*, 4967.
(51) Bar, G.; Brandsch, R.; Whangbo, M.-H. *Langmuir* **1998**, *14*, 7343.
(52) Bar, G.; Thomann, Y.; Brandsch, R.; Cantow, H.-J.; Whangbo, M. H. *Langmuir* **1997**, *13*, 3807.
(53) Magonov, S. N.; Elings, V.; Papkov, V. S. *Polymer* **1997**, *38*, 297.
(54) Feng, J.; Winnik, M. A.; Shivers, R. A.; Clubb, B. *Macromolecules* **1995**, *28*, 7671.
(55) Wang, Y.; Anderson, C. *Macromolecules* **1999**, *32*, 6172.
(56) Dinsmore, A. D.; Yodh, A. G. *Langmuir* **1999**, *15*, 314.

MA000221P